J. Fluid Mech. (2012), *vol.* 706, *pp.* 560–570. © Cambridge University Press 2012
doi:10.1017/jfm.2012.281

Micro-splashing by drop impacts

S. T. Thoroddsen[1]†, K. Takehara[2] and T. G. Etoh[2]

[1] Division of Physical Sciences and Engineering and Clean Combustion Research Center, King Abdullah University of Science and Technology (KAUST), Thuwal 23955-6900, Saudi Arabia

[2] Department of Civil and Environmental Engineering, Kinki University, Higashi-Osaka 577-8502, Japan

(Received 22 March 2012; revised 12 May 2012; accepted 8 June 2012;
first published online 18 July 2012)

We use ultra-high-speed video imaging to observe directly the earliest onset of prompt splashing when a drop impacts onto a smooth solid surface. We capture the start of the ejecta sheet travelling along the solid substrate and show how it breaks up immediately upon emergence from the underneath the drop. The resulting micro-droplets are much smaller and faster than previously reported and may have gone unobserved owing to their very small size and rapid ejection velocities, which approach 100 m s^{-1}, for typical impact conditions of large rain drops. We propose a phenomenological mechanism which predicts the velocity and size distribution of the resulting microdroplets. We also observe azimuthal undulations which may help promote the earliest breakup of the ejecta. This instability occurs in the cusp in the free surface where the drop surface meets the radially ejected liquid sheet.

Key words: aerosols/atomization, breakup/coalescence, drops

1. Introduction

The splashing of drops impacting onto solid surfaces is ubiquitous in nature and is also important in numerous industrial applications, among which are spray coating, cleaning and cooling (Yarin 2006). In some situations, such as spray combustion, splashing can be beneficial by forming out new surface area, while in many others it leads to detrimental outcomes, e.g. cross-contamination or uneven coating. The liquid breakup can occur through so-called 'prompt splashing' by the formation of fingers on the thin liquid sheet ejected radially along the solid (Thoroddsen & Sakakibara 1998; Rioboo *et al.* 2001), or from the breakup of a separated crown (Mundo, Sommerfeld & Tropea 1995; Yarin & Weiss 1995; Vander Wal, Berger & Mozes 2006; Roisman, Horvat & Tropea 2006). Prompt splashing is influenced by the roughness of the surface as well as by the surrounding gas pressure (Xu *et al.* 2005, 2007). The numbers and sizes of splashed droplets are of interest as they influence the production of aerosols from solute solutions, such as sea-water, when the solvent evaporates. This can affect diverse phenomena from cloud formation to public health.

Herein we use ultra-high-speed video imaging to show that the earliest prompt splashing may be promoted by capillary instability in the cusp-like crease which forms in the liquid's surface between the drop and the thin ejecta moving along the substrate. This may help break up the front into fast-moving micro-droplets smaller than previously observed, a phenomenon we call 'micro-splashing'.

† Email address for correspondence: sigurdur.thoroddsen@kaust.edu.sa

https://doi.org/10.1017/jfm.2012.281 Published online by Cambridge University Press

2. Experimental setup

We use gravity-driven water drops of diameter $D \simeq 5.5$ mm, where the impact velocity U is varied by changing the release height H, to as high as 1.7 m. This generates impact velocities up to 5.5 m s^{-1}. The Reynolds and Weber numbers of the impact are defined as $Re = \rho UD/\mu$ and $We = \rho DU^2/\sigma$, where the μ and ρ are the dynamic viscosity and density of the liquid and σ is the surface tension. We study We numbers up to 2480, while the Re takes values as high as 3.0×10^4. For reference, the impact of a large raindrop produces parameter values of $We \sim 5000$ and $Re \sim 30\,000$, thus encompassing the largest impact velocity studied herein (Villermaux & Bossa 2009). The effects of inertia, surface tension and viscous stress are often combined in the so-called splashing parameter (Mundo *et al.* 1995), $K = We\sqrt{Re} = \sqrt{\rho^3 D^3 U^5/(\sigma^2\mu)}$.

Figure 1(*a*) shows a schematic of the imaging setup. The impact was viewed through a glass plate which acts as the solid substrate. Each impact used a new clean uncoated microscope slide from Toshinriko Co. Ltd, but impacts on acrylic plates show similar results. Typical root-mean-square roughness of such slides is a few nanometres. We thereby conclude that the surface roughness plays no role in the splashing. To capture the rapid jetting motions, we use an ultra-high-speed CCD video camera (Etoh *et al.* 2003), at frame rates up to 1000 000 f.p.s. In contrast with regular high-speed CMOS video cameras, where the pixel area reduces with higher frame rates, here each frame contains 260×312 pixels, irrespective of the frame rate used. The pixel size is 63 μm, with fill factor of ∼15 % to accommodate the ISIS frame storage within the CCD chip. Direct lighting from a cool 350 W metal halide lamp (Sumita 350M) was used in combination with a long-distance microscope (Leica APO-Z16), at magnifications up to 18.4. The numerical aperture of the lens is as large as 0.224 NA, giving a minimum optically resolvable structural width of 0.74 μm. For observations under the drop we use the drop itself as a lens, to produce a spotlight of sufficient intensity for the highest frame rates, as sketched in figure 1(*a*).

3. Results

3.1. *First contact, fingering and azimuthal neck undulations*

The sequence of video frames in figure 1(*d*) shows the early contact of the drop with the glass plate, which occurs along a ring, entrapping a disc of air under the centre of the drop. This disc contracts rapidly by surface tension, into a central bubble (Thoroddsen *et al.* 2005; Mani, Mandre & Brenner 2010; Driscoll & Nagel 2011; Kolinski *et al.* 2012; van der Veen *et al.* 2012). The outer contact line is initially smooth, but immediately breaks up into fingerlike jets when the axisymmetric jet emerges. In figure 1(*d*) jetting starts at 10 μs after first contact (see the lower curves in figure 3(*b*) and supplementary video 1). Single-image flash photography (figure 1*b*) has previously shown the early onset of these fingers as smeared streaks (Thoroddsen & Sakakibara 1998; Thoroddsen *et al.* 2005), but our 1 μs exposure also reveals a regular azimuthal surface pattern (close-up in figure 1*e*), which sits in the free surface cusp between the emerging axisymmetric jet and the downward-moving drop surface, as sketched in figure 1(*f*). Figure 1(*c*) shows another example of these azimuthal patterns, which are quite regular along the periphery, indicating an underlying capillary instability mechanism. In figure 1(*f*) we sketch the proposed cusp or crease in the free surface. If the cusp is sharp enough it will intuitively not be a minimal surface and can thereby support an instability, as sketched in figure 2. We speculate that these neck undulations are imprinted onto the earliest emerging jet, promoting the

https://doi.org/10.1017/jfm.2012.281 Published online by Cambridge University Press

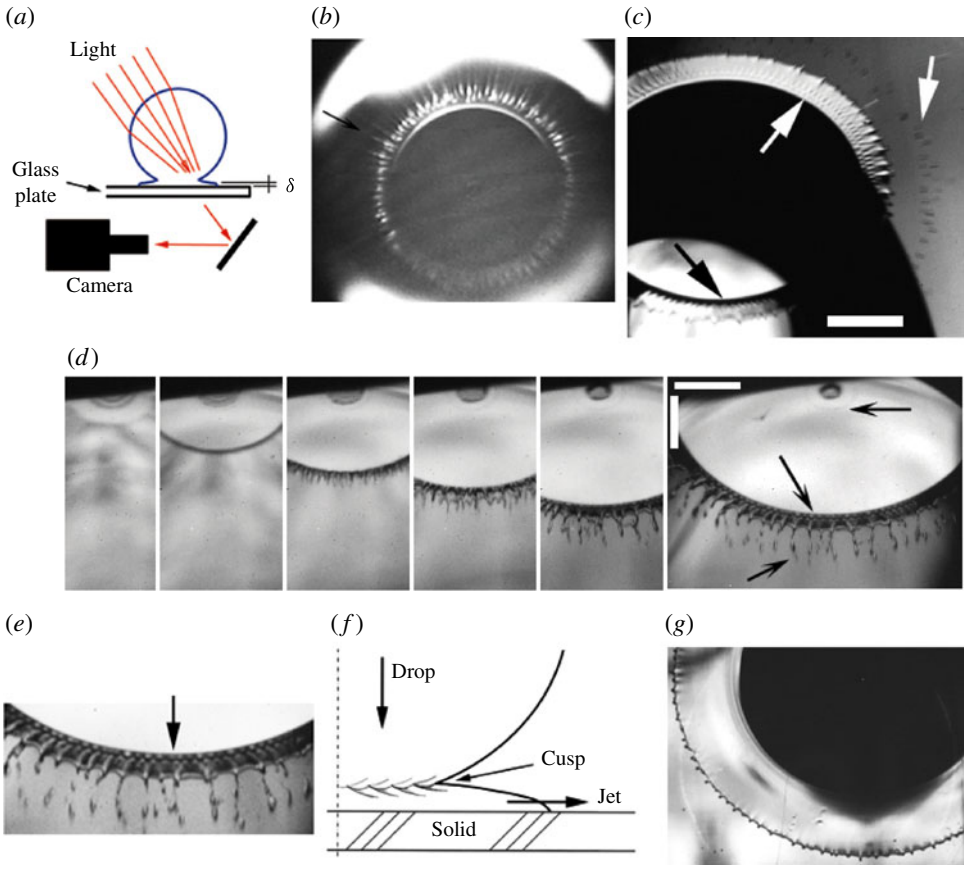

FIGURE 1. Observing the initial contact dynamics and micro-splashing. (*a*) Sketch of the optical setup. The impact is viewed through a glass substrate. The drop acts as a lens to intensify the illumination. (*b*) Snapshot from Thoroddsen & Sakakibara (1998) revealing smeared streaks. (*c*) Undulations on the ejecta (left arrows) and ejected droplets (rightmost arrow), shown at $t = 72$ μs after impact. The scale bar is 1 mm. (*d*) Direct observation of the instability at the base of the fingers, for $H \simeq 75$ cm ($Re = 20\,200$, $We = 1020$). The frames are taken from a 500 000 f.p.s. video sequence and shown 2, 8, 16, 24, 34 and 40 μs after the first contact. The arrows (from top to bottom) point to the faint ring of microbubbles left at the edge of the entrapped air disc, the undulations in the neck region and the fingers shedding droplets. The scale bars are both 500 μm long, owing to the slightly oblique view. See also supplementary video 1 available at journals.cambridge.org/flm. (*e*) Close-up image of the azimuthal instability, showing 32 regular undulations (arrow). (*f*) Sketch identifying the cusp in the free surface, location of the instability. (*g*) Fingers further along during the spreading.

fingers and forcing the onset of micro-splashing. While the classical cylindrical jet and drop are stable to azimuthal undulations, our geometry of a sharp cusp can support the proposed azimuthal undulations, as is shown schematically in figure 2, while continuity can be satisfied through vertical deformations of the air troughs.

These azimuthal undulations in the neck region are often obscured by shadows, and can only be counted under certain lighting conditions, as in figures 1(*c–e*) and 4(*a*). Figure 3(*a*) compares the number of the undulations to the number of the primary fingers which develop later on the edge of the jet, for larger spreading radii (see

https://doi.org/10.1017/jfm.2012.281 Published online by Cambridge University Press

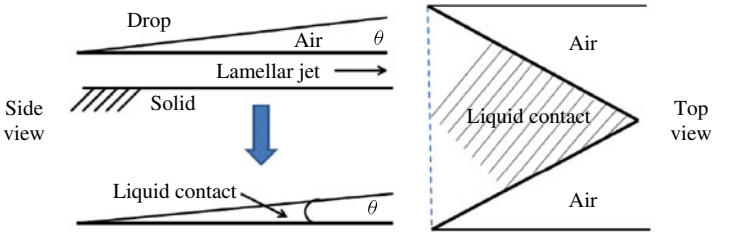

FIGURE 2. Schematic of zig-zag undulations in the sharp cusp between the drop and the jet. If θ is sharp enough, the surface area reduces for this contact shape between the drop and jet.

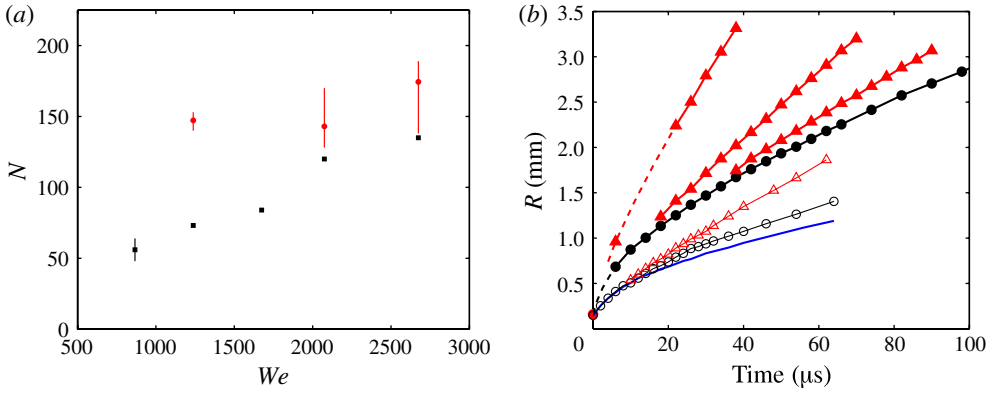

FIGURE 3. (*a*) Characterization of the azimuthal instability. Number of fingers (■) and initial azimuthal undulations in the cusp region (red ○), including the range of the handful of measurements. (*b*) Early contact between the drop and the substrate. The curves show the initial growth of the liquid jet's contact with the solid surface (-◯-) and the trajectory of typical ejected droplets (-△-). For the two impact velocities, $Re = 29\,700$, $We = 2200$ (filled symbols) and $Re = 19\,800$, $We = 980$ (open symbols). The blue line shows the radial location of the cusp between the drop and the ejecta sheet, for the latter case. The drop diameter $D \simeq 5.5$ mm, in both cases.

figure 1*g*). It shows clearly that the initial instability does not occur at the same wavelength as the final fingering pattern, which is for example observed for inkblots on paper (Marmanis & Thoroddsen 1996), where the deceleration of the expanding edge plays a role. Keep in mind that the fingers are prone to splitting and merging with neighbouring fingers (Thoroddsen & Sakakibara 1998) before the splat reaches its maximum extent. The number of late-stage fingers on the jet shows a uniform increase with *We*, whereas the number of initial azimuthal undulations is nearly constant over a range of *We*, which supports a geometric factor determining their wavelength. The relative constancy of these undulations supports our contention that the initial azimuthal instability is promoted in the free-surface cusp and not formed on a thicker edge of the initially axisymmetric jet. We propose that the initial thickness of the jet, as it emerges from the base of the drop, is governed by the viscous boundary layer along the flat plate (Haller *et al.* 2002; Xu 2010). Note that our impact Reynolds numbers are larger than those in De Ruiter, Pepper & Stone (2010). In combination with the unsteady nature of the flow, this leads to a jet thickness

https://doi.org/10.1017/jfm.2012.281 Published online by Cambridge University Press

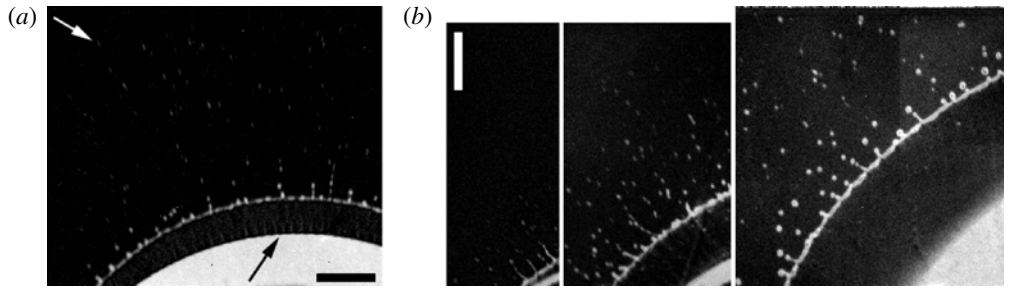

FIGURE 4. Ejected micro-droplets. The droplets are highlighted by using image differences, to minimize the effects of image blemishes. (*a*) Micro-droplets (white arrow) and azimuthal undulations on the jet surface (black arrow), taken from a 1 million f.p.s. video sequence (supplementary video 2). (*b*) Video frames showing breakup of early fingers emerging from the front of the jet and the continuing ejection of progressively larger micro-droplets. $Re = 30\,900$, $We = 2380$ for both cases. The times between the frames are 22 and 64 μs. The scale bars are both 0.5 mm.

of $\delta \simeq \sqrt{\nu T}$, where ν is the liquid kinematic viscosity and T is the time from first contact. For the lower curves in figure 3(*b*), $T \simeq 10$ μs, giving a thickness $\delta \simeq 3$ μm. This jet thickness would reduce with increased impact velocity and We, producing shorter azimuthal instability wavelengths, but not remain constant as is observed. Furthermore, the maximum number of observed undulations in the cusp reaches ∼190 here. This corresponds to an initial azimuthal wavelength of ∼45 μm, which is more than $10 \times \delta$, i.e. significantly larger than the most unstable Rayleigh wavelength of the edge of the jet. Once the jet has moved significantly ahead of the cusp, it leaves a standing capillary wave which decays away as the cusp is blunted by the changing geometry (see figure 1*c* and supplementary video 5).

By changing the impact height, we have identified the critical impact velocity, where micro-splashing begins. For our water drops this occurs for $H \simeq 35$ cm, which corresponds to $Re = 14\,300$, $We = 510$ and $K = 60\,900$. Slightly above this critical value, the original splashing is associated with regularly spaced droplets, of near-uniform size as is evident in figure 1(*c*). For higher impact velocities the micro-splashing becomes more random and proceeds during the spreading, producing a range of droplet sizes and velocities.

3.2. *Micro-splashing*

For larger values of K the initial emergence of the jet generates the finest droplets which are ejected at the highest speeds. Subsequently, the sheet continues to fragment, releasing progressively larger droplets but at lower velocities. This feature of the micro-splashing is clearly visible in the frames in figure 4(*b*) and supplementary video 2.

The radial spreading of the jet can be tracked from videos, as is done in figure 3(*b*). The radial motion of the tip of the jet is reasonably modelled by a power-law $R \sim t^{1/2}$. However, minor deviations should be expected, as droplets are continually shed from the edge of the jet, thereby reducing its length. Furthermore, at the large We used herein the drop is deformed away from spherical shape due to air resistance, thereby directly introducing effects owing to the impact height and droplet phase of oscillation as it hits the plate. These effects will inevitably cause slight deviations from this power-law.

https://doi.org/10.1017/jfm.2012.281 Published online by Cambridge University Press

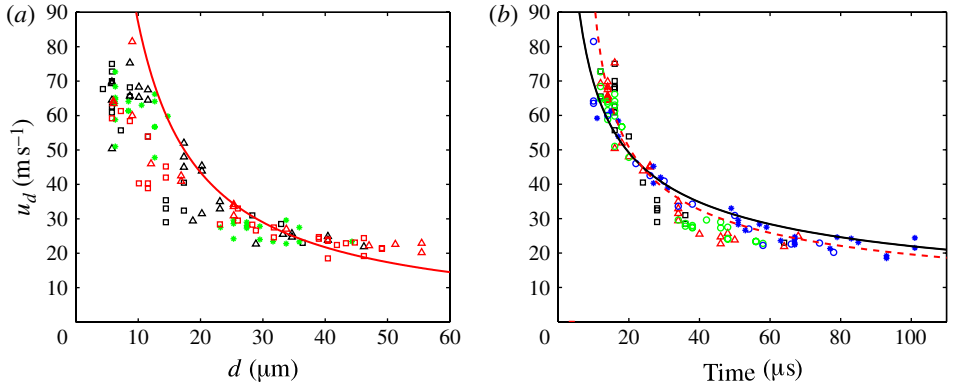

FIGURE 5. Characterization of the micro-droplet ejection velocities. (*a*) Velocity of droplets versus size for the largest impact height, $Re \simeq 2.9 \times 10^4$. The red line is from (3.1) with $C = 4$. (*b*) Velocity versus time from first contact, for five realizations. The solid line is the fit $u_d \sim t^{-0.5}$ and the broken line $u_d \sim (t - t_o)^{-0.5}$, where $t_o = 6$ μs, to account for the original start of jetting.

The micro-droplets emerge at the velocity of the decelerating sheet, i.e. tangentially to the curves tracking the motion of the front in figure 3(*b*). For the dotted curve the earliest measured droplet velocity is ∼80 m s^{-1}. This is an order of magnitude larger than the corresponding Taylor–Culick velocity of a liquid edge being pulled back by surface tension, which is $u_{TC} = \sqrt{2\sigma/(\rho\delta)} \simeq 7$ m s^{-1}. This ejecta speed occurs for the highest drop impact velocity ($U \sim 5.5$ m s^{-1}), and the time resolution of the videos is not sufficient to freeze the earliest motions (supplementary videos 3 and 4), top curves in figure 3(*b*). However, for the lower impact velocity (lower curves), we can track the growth of the contact area until the ejecta emerges after ∼10 μs from first contact (see also supplementary video 1). The earlier the droplets separate from the front, the faster and smaller they are. We characterize this effect in figure 5(*a*), which shows the droplet ejection velocity versus droplet size. This is done using numerous realizations at the largest impact velocity ($H = 1.65$ m), corresponding to $Re = 29\,700$. Here, the droplets are shed until the jet reaches $r \simeq 1.1\times$ drop radius.

Since the droplets emerge from the tip of the sheet approximately tangentially to its motion in figure 3(*b*), their velocity is therefore the same as the local jet velocity $u_d \propto \mathrm{d}R/\mathrm{d}t \sim t^{-1/2}$, whereas the droplet size d can be estimated by the thickness of this jet. This thickness grows through viscous effects, as $d \sim \delta \simeq C\sqrt{\nu t}$. This gives us a relationship between the micro-droplets' splashing velocity and their size, i.e. after normalizing the time t by D/U,

$$u_d \simeq C\frac{\sqrt{\nu DU}}{d}, \tag{3.1}$$

which qualitatively fits the data in figure 5(*a*), with $C \simeq 4$. We note that there is however a significant range of observed velocities for each droplet size, while the fastest velocities for each droplet size clearly follow the trend in (3.1). This spread in the data arises principally due to formation of satellite droplets as the larger drops break away from the front, thereby producing some smaller but slower-moving droplets, sitting below the curve. Therefore, the data show better collapse if we plot velocity versus time from impact, as is done in figure 5(*b*). The data follow the above

https://doi.org/10.1017/jfm.2012.281 Published online by Cambridge University Press

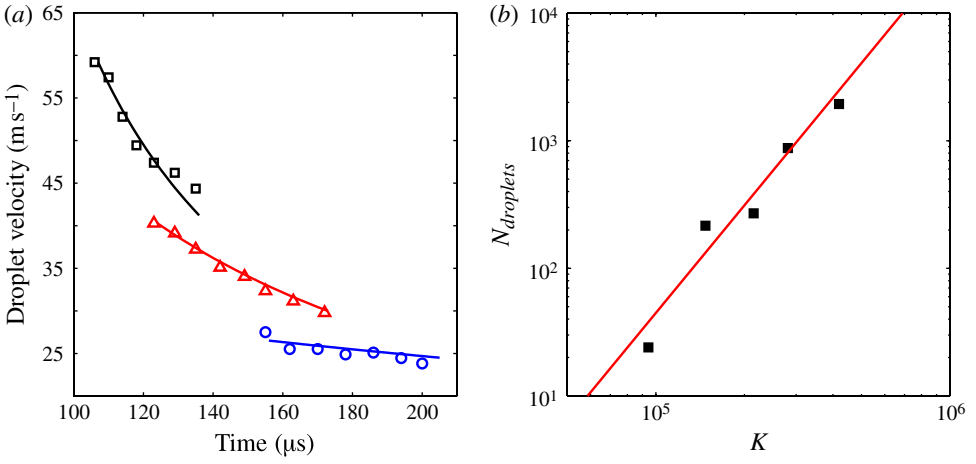

FIGURE 6. (*a*) Deceleration of the ejected micro-droplets due to air drag. Data for droplet diameters d of ∼8 (□), 12 (△), and 32 μm (◯). The curves are calculated using $C_D \simeq 1.9$. (*b*) Total number of splashing droplets, plotted versus the splashing parameter. The solid line has a slope of 14/5.

relation $u_d \sim t^{-1/2}$ reasonably well. Keep in mind that the velocities of the earliest droplets are measured as they enter the field of view of the camera and have not been extrapolated towards the point of emergence, which would give slightly larger velocities for the smallest droplets.

3.3. *Micro-droplet deceleration*

Figure 6(*a*) shows in-flight deceleration of three typical micro-droplets of different sizes. Here we have accurately modelled the deceleration using form drag, with a drag coefficient $C_D = 1.9$, which is justified as the drop $Re \sim 10^2$. The smallest droplet decelerates by 30 % in only 40 μs. Keep in mind that this is only an approximate drag model, as C_D is a $f(Re)$, and there must be some surrounding air flow away from under the centre of the impacting drop as it hits the substrate. This parallel air velocity cannot been measured here, but will reduce the drag force. The presence of the solid surface, on which the droplets hydroplane, will also modify C_D. The smallest droplets decelerate the most, as

$$\frac{\mathrm{d}u_d}{\mathrm{d}t} = \frac{-3C_D}{4}\left(\frac{\rho_{air}}{\rho_{liq}}\right)\frac{u_d^2}{d} \propto \frac{1}{d}. \tag{3.2}$$

The larger droplets or even the jet front itself can therefore, later on, overtake the rapidly decelerating smallest micro-droplets. However, the surrounding air flow can also easily levitate or suspend the smallest droplets, as the terminal velocity of a 10 μm drop, in free fall under gravity, is only ∼10 mm s^{-1}. In other words, the smallest droplets are here ejected at ∼10^4 times their terminal velocity.

3.4. *Number of micro-droplets*

The total number of splashed micro-droplets N_{tot} grows rapidly with increasing Re. Figure 6(*b*) shows that this number scales approximately as a power-law with the splashing parameter K. A simple dimensional argument suggests that the total number of micro-droplets is proportional to the area of the jet which breaks into droplets.

https://doi.org/10.1017/jfm.2012.281 Published online by Cambridge University Press

The size of this area is area $\sim (U_j \times t^*)^2$, where $U_j \sim U\sqrt{Re}$ is the original ejecta velocity of the jet (Thoroddsen 2002; Eggers *et al.* 2010). The time t^* identifies the time at which the front stops breaking up into droplets. To determine this time t^* we note that the Weber number of the jet $We_\delta = \rho\delta U_j^2/\sigma$ must reduce below a certain critical number, where surface tension prevents breakup of the front. Using the earlier time-scaling for $\mathrm{d}R/\mathrm{d}t \sim t^{-1/2}$, we see that We_δ reduces with time, as

$$We_\delta \sim \frac{\rho\sqrt{\nu t}Ret^{-1}}{\sigma} \sim \frac{\rho UD}{\sigma\sqrt{\nu t}}. \tag{3.3}$$

Solving for t^* we get $t^* \sim (\rho DU)^2/(\nu\sigma^2)$, and the area and total number of splashed micro-droplets become

$$N_{tot} \propto \text{area} \sim (U_j \times t^*)^2 \sim U^7 \sim K^{14/5}. \tag{3.4}$$

This model contains a number of speculative assumptions which need further experimental verification. However, it is in qualitative agreement with the data in figure 6(*b*).

4. Discussion and conclusions

The impact velocities studied herein are small enough that the jetting is not produced by liquid compressibility (Lesser & Field 1983), as the Mach number is quite low, i.e. $M = U/c < 0.004$, based on the speed of sound in water, $c \sim 1500$ m s^{-1}. This is also clear from the jetting time produced by compressibility, which in the acoustic limit can be estimated as $t_j = DU/(4c^2) \simeq 3$ ns (Haller *et al.* 2002; Haller, Ventikos & Poulikakos 2003). Another measure of the significance of compressibility is the time it takes the initial shock, produced by contact, to reach the top of the drop, i.e. $t_D = D/c \simeq 3$ μs. The emergence of the jetting at 10 μs after the first contact, in figure 3(*b*), is therefore not related to the initial shock wave which arises from the first contact. In other word, the entire drop of liquid knows about the contact long before the jetting begins.

Recent work by Rein & Delplanque (2008) proposes that air entrainment at the moving contact line is responsible for the fingering. Our results do not show entrainment of air bubbles under the original front, where it moves at the highest speed. Furthermore, our proposed instability is not at the contact line but rather at the free-surface cusp. However, secondary prompt splashing may take place later on during the spreading (Rioboo *et al.* 2001; Xu *et al.* 2005). Supported by the large variability in previous data collated by Rein & Delplanque (2008), our results reinforce the view that there may be a number of different drop-splashing mechanisms at play, which collectively will resist any overarching universal scaling, such as a K-parameter (Zhang *et al.* 2010; Krechetnikov & Homsy 2009).

Our images show that the initial instability and ejection of fast-moving droplets occurs spontaneously when the jet emerges. Therefore, we expect the resulting distribution of droplet sizes and velocities for this micro-splashing to be fundamentally different from the various other proposed splashing mechanisms, such as rim instability (Roisman *et al.* 2006; Villermaux & Bossa 2011), crown breakup (Zhang *et al.* 2010; Xu *et al.* 2005), levitated viscous sheets (Thoroddsen, Takehara & Etoh 2010; Driscoll, Stevens & Nagel 2010) or ejecta sling-shots (Thoroddsen *et al.* 2011). Direct comparison of droplet sizes is difficult as our resolution is much finer than in previous studies. Keep in mind that all the micro-droplets observed in our experiments are less than half the size of the finest drops resolved by the paper blotting method

https://doi.org/10.1017/jfm.2012.281 Published online by Cambridge University Press

($d > 100$ μm) employed by Xu *et al.* (2007), where they erect a paper-sheet outside the edge of the splash to catch the flying droplets. Our observations can therefore complement these results with prompt splashing at the very earliest times. The strong deceleration of the smallest droplets, by air drag, would also not allow the blotting method to work effectively.

What selects the wavelength of the cusp instability? The free-surface cusp forms when the jetting starts. Therefore the sharpness of the corner of the cusp is determined by geometry as well as by competition between blunting by surface tension and sharpening by the downward motion of the drop surface, as was sketched in figure 1(*f*). This balance suggests a critical value of the *We* below which the cusp is simply blunted by surface tension (Oguz & Prosperetti 1989; Cresswell & Morton 1995). However, our modelling of this instability and early breakup suffers from the fact that our imaging cannot directly observe the sharpness of the cusp. To apply the Rayleigh instability to a cylindrical void within a liquid, one needs the radius of curvature blunting the cusp, R_{cusp}, to predict the fastest growing azimuthal wavelength $\lambda_{cusp} = (2\pi/0.484)R_{cusp}$. For surface tension to drive the cusp outwards, this characteristic curvature must be such that $R_{cusp} < \sigma/(\rho U^2)$, which for a typical radial velocity of the cusp of 10 m s^{-1} gives $R_{cusp} \leqslant 0.7$ μm and $\lambda_{cusp} < 9$ μm, which is significantly smaller than the observations of ∼50 μm. For the highest impact velocities the cusp moves radially at speeds where the cusp would require curvatures sharper than the critical capillary-viscous scale $R_\star = 2\mu^2/(\rho\sigma)$, where viscous stress balances surface tension no matter how sharp the cusp. We conclude that the inertial inviscid dynamics are driving the radial motion of the cusp and not the surface tension, in contrast to coalescence-driven motions. The capillary instability therefore rides on top of this inviscid geometry. Lubrication pressure in the air may also play a role here: see Eggers (2001). To verify that these observed undulations play the proposed role in destabilizing the emerging jet, even faster imaging will be needed. Experiments showing micro-splashing under reduced air pressure would also support its geometric nature.

Herein we have presented direct video imaging of the earliest prompt splashing, which we call ‘micro-splashing’. The imaging identifies an instability in the crease in the free surface, where the drop meets the thin jet travelling along the solid substrate. This micro-splashing occurs during the initial contact and differs markedly from the typical splashing through crown breakup (Rioboo *et al.* 2001; Roisman *et al.* 2006; Villermaux & Bossa 2011; Xu *et al.* 2005), for example by producing much smaller droplets. At lower magnifications and slower frame rates, used in most earlier studies, these minute and fast-moving droplets can smear, becoming effectively invisible. Furthermore, as the smallest micro-droplets $d \sim 5$ μm are ∼1/1000 smaller than the original drop size, these results present significant challenges to numerical simulations of this process, not only due to the large range of scales, but also from the fundamentally three-dimensional nature of the instability (Tryggvason, Scardovelli & Zaleski 2011). The largest impact velocities produce a myriad of micron-sized droplets, potentially having great effect on aerosol production from solutes such as sea-water, thereby being of importance to climate and public health.

Acknowledgements

S.T.T. was partially supported by KAUST GCR AEA Grant 70000000028 (Fine-Resolution Printing).

https://doi.org/10.1017/jfm.2012.281 Published online by Cambridge University Press

Supplementary videos

Supplementary videos are available at journals.cambridge.org/flm.

REFERENCES

CRESSWELL, R. W. & MORTON, B. R. 1995 Drop-formed vortex rings – the generation of vorticity. *Phys. Fluids* **7**, 1363–1370.

DRISCOLL, M. M. & NAGEL, S. R. 2011 Ultrafast interference imaging of air in splashing dynamics. *Phys. Rev. Lett.* **107**, 154502.

DRISCOLL, M. M., STEVENS, C. S. & NAGEL, S. R. 2010 Thin film formation during splashing of viscous liquids. *Phys. Rev.* E **83**, 036302.

EGGERS, J. 2001 Air entrainment through free-surface cusps. *Phys. Rev. Lett.* **86**, 4290–4293.

EGGERS, J., FONTELOS, M. A., JOSSERAND, C. & ZALESKI, S. 2010 Drop dynamics after impact on a solid wall: theory and simulations. *Phys. Fluids* **22**, 062101.

ETOH, T. G., POGGEMANN, D., KREIDER, G., MUTOH, H., THEUWISSEN, A. J. P., RUCKELSHAUSEN, A., KONDO, Y., MARUNO, H., TAKUBO, K., SOYA, H., TAKEHARA, K., OKINAKA, T. & TAKANO, Y. 2003 An image sensor which captures 100 consecutive frames at 1000000 frames/s. *IEEE Trans. Electron Devices* **50**, 144–151.

HALLER, K. K., VENTIKOS, Y., POULIKAKOS, D. & MONKEWITZ, P. 2002 Computational study of high-speed liquid droplet impact. *J. Appl. Phys.* **92**, 2821–2828.

HALLER, K. K., VENTIKOS, Y. & POULIKAKOS, D. 2003 Wave structure in the contact line region during high speed droplet impact on a surface: solution of the Riemann problem for the stiffened gas equation of state. *J. Appl. Phys.* **93**, 3090–3097.

KOLINSKI, J. M., RUBINSTEIN, S. M., MANDRE, S., BRENNER, M. P., WEITZ, D. A. & MAHADEVAN, L. 2012 Skating on a film of air: drops impacting on a surface. *Phys. Rev. Lett.* **108**, 074503.

KRECHETNIKOV, R. & HOMSY, G. M. 2009 Crown-forming instability phenomena in the drop splash problem. *J. Colloid Interface Sci.* **331**, 555–559.

LESSER, M. & FIELD, J. E. 1983 The impact of compressible liquids. *Annu. Rev. Fluid Mech.* **15**, 97–122.

MANI, M., MANDRE, S. & BRENNER, M. P. 2010 Events before droplet splashing on a solid surface. *J. Fluid Mech.* **647**, 163–185.

MANDRE, S. & BRENNER, M. P. 2012 The mechanism of a splash on a dry solid surface. *J. Fluid Mech.* **690**, 148–172.

MARMANIS, H. & THORODDSEN, S. T. 1996 Scaling of the fingering pattern of an impacting drop. *Phys. Fluids* **8**, 1344–1346.

MUNDO, C., SOMMERFELD, M. & TROPEA, C. 1995 Droplet–wall collisions: experimental studies of the deformation and breakup process. *Intl J. Multiphase Flow* **21**, 151–173.

OGUZ, H. N. & PROSPERETTI, A. 1989 Surface-tension effects in the contact of liquid surfaces. *J. Fluid Mech.* **203**, 149–171.

REIN, M. & DELPLANQUE, J.-P. 2008 The role of air entrainment on the outcome of drop impact on a solid surface. *Acta Mech.* **201**, 105–118.

RIOBOO, R., TROPEA, C. & MARENGO, M. 2001 Outcomes from a drop impact on solid surfaces. *Atomiz. Sprays* **11**, 155–165.

ROISMAN, I. V., HORVAT, K. & TROPEA, C. 2006 Spray impact: rim transverse instability initiating fingering and splash and description of a secondary spray. *Phys. Fluids* **18**, 102104.

DE RUITER, J., PEPPER, R. E. & STONE, H. A. 2010 Thickness of the rim of an expanding lamella near the splash threshold. *Phys. Fluids* **22**, 022104.

THORODDSEN, S. T. 2002 The ejecta sheet generated by the impact of a drop. *J. Fluid Mech.* **451**, 373–381.

THORODDSEN, S. T., ETOH, T. G., TAKEHARA, K., OOTSUKA, K. N. & HATSUKI, Y. 2005 The air bubble entrapped under a drop impacting on a solid surface. *J. Fluid Mech.* **545**, 203–212.

THORODDSEN, S. T. & SAKAKIBARA, J. 1998 Evolution of the fingering pattern of an impacting drop. *Phys. Fluids* **10**, 1359–1374.

https://doi.org/10.1017/jfm.2012.281 Published online by Cambridge University Press

THORODDSEN, S. T., TAKEHARA, K. & ETOH, T. G. 2010 Bubble entrapment through topological change. *Phys. Fluids* **22**, 051701.

THORODDSEN, S. T., THORAVAL, M.-J., TAKEHARA, K. & ETOH, T. G. 2011 Droplet splashing by a sling-shot mechanism. *Phys. Rev. Lett.* **106**, 034501.

TRYGGVASON, G., SCARDOVELLI, R. & ZALESKI, S. 2011 *Direct Numerical Simulations of Gas–Liquid Multiphase Flows*. Cambridge University Press.

VAN DER VEEN, R. C. A., TRAN, T., LOHSE, D. & SUN, C. 2012 Direct measurements of air layer profiles under impacting droplets using high-speed colour interferometry. *Phys. Rev.* E **85**, 026315.

VANDER WAL, R. L., BERGER, B. M. & MOZES, S. D. 2006 The splash/non-splash boundary upon a dry surface and thin fluid film. *Exp. Fluids* **40**, 23–32.

VILLERMAUX, E. & BOSSA, B. 2009 Single-drop fragmentation determines size distribution of raindrops. *Nature Phys.* **5**, 697–702.

VILLERMAUX, E. & BOSSA, B. 2011 Drop fragmentation on impact. *J. Fluid Mech.* **668**, 412–435.

XU, L. 2010 Instability development of a viscous liquid drop impacting a smooth substrate. *Phys. Rev.* E **82**, 025303.

XU, L., BARCOS, L. & NAGEL, S. R. 2007 Splashing of liquids: interplay of surface roughness with surrounding gas. *Phys. Rev.* E **76**, 066311.

XU, L., ZHANG, W. W. & NAGEL, S. R. 2005 Drop splashing on a dry smooth surface. *Phys. Rev. Lett.* **94**, 184505.

YARIN, A. L. & WEISS, D. A. 1995 Impact of drops on solid surfaces: self-similar capillary waves, and splashing as a new type of kinematic discontinuity. *J. Fluid Mech.* **283**, 141–173.

YARIN, A. L. 2006 Drop impact dynamics: splashing, spreading, receding, bouncing... *Annu. Rev. Fluid Mech.* **38**, 159–192.

ZHANG, L. V., BRUNET, P., EGGERS, J. & DEEGAN, R. D. 2010 Wavelength selection in the crown splash. *Phys. Fluids* **22**, 122105.

https://doi.org/10.1017/jfm.2012.281 Published online by Cambridge University Press